JOURNAL OF MATERIALS SCIENCE 25 (1990) 2754–2764

The physics and chemistry of the sintering of silicon

WILLIAM S. COBLENZ
Norton Company, Advanced Ceramics Division, Northboro, Massachusetts 01532, USA

Silicon is a model material for studying the sintering of covalently bonded non-oxide ceramics. The sintering of silicon has direct applications as well to polycrystalline photovoltaics and the reaction sintering of silicon nitride. Surface diffusion is found to be the dominant mass transport path for pure silicon of all particle sizes of interest. Both boron and oxygen are surface-active and effective in inhibiting surface transport, thereby allowing shrinkage to occur by either grain-boundary or lattice diffusion.

1. Introduction

The sintering of silicon is of interest because silicon is a model material for other covalently bonded non-oxide ceramics. The near-net shape-forming capability associated with pressureless sintered silicon is also applicable to non-planar silicon devices where the polycrystalline shaped body can be converted to an oriented single crystal using a modified Bridgeman crystal growth technique.

Our understanding of silicon sinterability begins in 1975 with the first studies of Greskovich and Rosolowski [1, 2]. They studied the sinterability of two types of silicon powder. Powder I was prepared by crushing high-purity single-crystal silicon followed by jet-milling to produce powders of 1.35 and 0.23 μm average particle sizes. Powder II was prepared by thermal decomposition of silane at 600 to 700° C, followed by an isothermal grain-growth anneal at 700° C. Powders of 0.06 and 0.18 μm average particle size were prepared by this method.

Compacts of silicon which did not densify at 1350° C showed a weight loss of 3 to 5%, leading the investigators to conclude that coarsening occurs by a vapour-phase mechanism. Also, from Herring's scaling laws, the time to gain a relative neck size (X/A) should vary inversely as the 4th, 4th, 3rd and 2nd power of the particle size for matter transport by grain-boundary diffusion, surface diffusion, lattice diffusion and evaporation–condensation, respectively. If, for intrinsic silicon, coarsening were by surface diffusion then reducing the particle size would have no effect for a competing grain-boundary diffusion mechanism and would increase coarsening if shrinkage were by lattice diffusion. For compacts of 1.9, 11, 14.6 and 44 $m^2 g^{-1}$ surface area, shrinkages (1 h, 1350° C, argon) were 1, 2.5, 8 and 23%, respectively, which suggests shrinkage is controlled by either lattice or grain-boundary diffusion and the competing coarsening mechanism is evaporation–condensation.

Greskovich [3] found that small amounts of boron enhanced the sinterability of silicon while small amounts of tin promoted coarsening. To be consistent with previous conclusions [1, 2] that vapour-phase transport was the predominant coarsening path for pure silicon, he concluded that boron increases and tin decreases the grain-boundary diffusion coefficient of silicon.

Haggerty and co-workers [4] have prepared high-purity, ultrafine ($> 60 m^2 g^{-1}$) silicon powders by laser-induced decomposition of silane. Sintering behaviour of these powders varied from batch to batch, some giving near full density, others only a few per cent shrinkage when sintered under the same conditions as used by Greskovich and Rosolowski. The use of argon-atmosphere glove boxes to eliminate air contact with the powder is one major difference between the work of Haggerty and the prior study of Greskovich [1, 2].

The conclusion of Greskovich and co-workers that vapour-phase transport dominated the coarsening of pure silicon came into question in 1981 with the surface diffusivity measurements of Robertson [5] and Coblenz [6]. These studies taken together showed that surface transport should dominate vapour-phase transport for pure silicon of all particle sizes studied.

Subsequent studies by Shaw and Heuer [7] and Möller and Welsch [8] recognized the contradiction between the vapour-phase coarsening assumption of Greskovich and co-workers [1–3] and the surface diffusivity measurements [5, 6] which followed. Shaw and Heuer suggested that vapour-phase coarsening dominated by SiO could account for the coarsening and weight losses and be consistent with the Herring's scaling laws results of Greskovich *et al.* [1, 2]. Möller and Welsch studied the sinterability of an ultrafine silane-derived silicon powder in a vacuum. They noted that green densities of greater than 42% of theoretical were required for densification. The surface regions of pellets which densified contained large pores and coarse grains (~ 1 μm) while the interior was generally fine-grained (0.05 to 0.3 μm) with fine porosity.

Munir [9] has derived analytical expressions for the role of oxide layers in the sintering of metals. Although Munir does not specifically discuss the sintering of

0022–2461/90 $03.00 + .12 © *1990 Chapman and Hall Ltd.*

silicon, silicon clearly falls into the category of a metal with a stable oxide and a low cation diffusivity in the oxide where an incubation period is associated with break-up of the oxide film at high temperature. This view is supported by the experience gained from the nitriding of silicon powder compacts [10].

Silica surface layers on silicon may be unstable in a high vacuum or reducing atmospheres due to the high vapour pressure of SiO. Hydrogen enhances the nitridation of silicon powders by reducing the surface oxide layer. Iron enhances the nitridability of silicon powders because it promotes the "devitrification and disruption of the protective silica film allowing the $SiO_{(g)}$ generated at the Si/SiO_2 interface to escape..." according to Boyer and Moulson [10]. They also state that "sintering of the silicon, which was found to be a feature of iron-free compacts was totally suppressed by the presence of even 55 ppm Fe" and that "Fe suppresses the sintering of silicon particles during argon-sintering or nitridation of the silicon powder compact". These authors use the term sintering to mean neck growth between particles, and no indication of whether or not shrinkage occurred was given.

The intention of this paper is to address the roles of oxygen and boron in the sintering of silicon. Experiments have been performed to determine the effect of these elements on surface transport and evaporation, with Auger spectroscopy used to document surface chemistry.

2. Experimental procedure

2.1. Materials

Model sintering experiments were performed using polycrystalline spheres (Texas Instruments Co.) of 150 to 250 μm diameter. The grain size of the spheres varied between 40 and 100 μm as measured on polished and etched sections. The spheres were macroscopically smooth with small pits observed at high magnification in the SEM. Prior to use, the spheres were washed in concentrated hydrofluoric acid followed by distilled water and electronic-grade acetone. Plates of silicon for use in sphere-plate sintering experiments, evaporation rate measurements, or grain-boundary grooving experiments, were either cut from: silicon [1 1 1] single crystals; polycrystalline silicon doped with 0.2 wt % boron (prepared by vacuum arc melting); or high-purity CVD polycrystalline boule.

2.2. Auger spectroscopy

A scanning Auger microprobe (Model 590-A, Physical Electronics Industries, Inc., Eden Prairie, MN) equipped with an argon sputtering gun for depth profiling and a spatial resolution of approximately 0.5 μm was used to document the surface chemistry.

Semi-quantitative analysis of the Auger spectra was performed using the procedures and elemental sensitivity factors from the Physical Electronics Handbook [11]. The high-energy silicon peak was used in these calculations because of its lower sensitivity to contamination layers. The peak-to-peak heights were divided by the elemental sensitivity factors to obtain the relative atomic abundance and normalized by the sum of the relative atomic abundances to arrive at the relative atom fractions. This procedure is most inaccurate for film thicknesses that are small relative to the electron escape depth.

2.3. Evaporation rate measurements

Evaporation rate measurements were made using both weight-loss and step-height techniques. Weight-loss measurements were made in a vacuum furnace (Model 1968, Richard D. Brew & Co. Inc., Concord, NH) equipped with a water-baffled oil diffusion pump, tantalum heating elements and molybdenum heat shields. Operating pressures of between 10^{-5} and 10^{-6} torr, measured in the chamber, were obtained at operating temperatures of up to 1350° C.

Samples were heat-treated in a molybdenum crucible. Crucibles were cleaned before use with acetone and heat-treated at ~2300° C in a vacuum before first use. A two-colour pyrometer with a close-up lens attachment was used for temperature measurement. Measurements were made by focusing into a 1/4 in. (6 mm) diameter black-body hole drilled into the molybdenum crucible.

Evaporation rates were calculated by dividing weight lost by the time at temperature and the exposed surface area. The exposed surface area was taken to be the sum of the top and side areas. The top area was determined from the sample thickness and mass, since the samples were irregularly shaped flat thin plates. The side area was determined from the thickness and perimeter. The error in measurement of the perimeter of the samples may have been as large as $\pm 10\%$, leading to errors in the calculated evaporation rate of $\pm 5\%$ since the side area amounted to half the total area for the small samples. The evaporation coefficient was determined from the ratio of the measured evaporation rate and the Knudsen evaporation rate calculated from JANAF table data [12].

Langmuir evaporation rates were also measured by the step height technique. The evaporation rate is calculated from the step on the sample created by masking part of the sample to prevent evaporation and thereby preserving a reference plane as the sample is heat-treated. Step heights were measured with a micro-Michelson interferometer (Carl Zeiss interference microscope).

The relative height differences between two fringes is $\lambda/2 = 0.2675\,\mu$m for the thallium illumination source used. Height differences as small as $\lambda/20 \approx 0.027\,\mu$m can be resolved for smooth surfaces of high reflectivity.

Samples were heat-treated in a tantalum strip heater in a bell-jar vacuum system. The tantalum foil was folded to provide a slot into which samples could be clamped in place. A hole in the foil adjacent to the sample allowed free evaporation to occur while the strip heater masked the rest of the sample. Temperature measurements were accomplished with a Pt/Pt–10% Rh thermocouple placed within an alumina thermocouple tube. The strip heater was wrapped around the thermocouple tube with the bead placed in the middle of the tube just below the position of the

sample. The bell-jar system was pumped with a vac-ion pump. The chamber was also equipped with a liquid nitrogen cryo-pump.

The temperature was controlled manually by means of a variable transformer. A surface instability observed for boron-doped samples resulted in a rough surface on which interference fringes were too diffuse to be used for height measurements. Facets which occasionally occurred on undoped and doped samples also limited the usefulness of the step-height technique. Evaporation of the boron-doped samples for extended time also resulted in boron-containing precipitates since boron has a much lower vapour pressure than silicon. Because weight loss measurements are insensitive to surface roughness, they were found to be more useful for investigating the effect of boron on the vapour transport of silicon.

2.4. Grain-boundary grooving experiments

Preliminary grain-boundary width measurements were made on samples used for step-height measurements. The bell-jar vacuum system with tantalum strip heater has been described in Section 2.3. Groove widths were measured with either the interference microscope or in a scanning electron microscope.

The Brew ® vacuum furnace, described in the section on evaporation rate measurements, was used for most of the grain-boundary grooving experiments. Molybdenum was found to be an acceptable crucible material for use with silicon although there was some reaction at points of contact.

Grain-boundary grooving experiments with boron-doped samples were complicated by evaporation of silicon in the vacuum which results in an increase in boron at the surface of the sample. A molybdenum foil-lined alumina tube furnace operated with titanium-gettered flowing argon worked best. Boron was segregated to the surface in what appeared to be near-equilibrium thin films, in contrast to samples heat-treated under active oxidation conditions which resulted in boron-depleted surface regions or samples heat-treated under conditions where excessive silicon evaporation leaves the surface boron enriched to a depth of several micrometres.

A Zeiss two-beam interference microscope, as described in Section 2.3, was used to obtain the grain-boundary groove profile. Grain-boundary widths were also estimated from SEM photomicrographs. Surface topography in the SEM is enhanced by using back-scattered electrons and a small tilt angle. This technique was developed by Dynys [13] for small groove widths. Boundary widths from the interference microscope were measured on pictures taken at a maximum magnification of 252×. Widths could be measured to ~0.1 mm accuracy with the aid of an ×8 magnifier. Grain-boundary width measurements thus have an accuracy of approximately 0.4 μm. Only those boundaries having symmetrical profiles were measured.

The grain-boundary groove width was used to calculate the surface diffusivity. According to Mullins [14], if grain-boundary grooving occurs by a surface diffusion mechanism, the groove width is given by

$$w = 4.6(Bt)^{1/4}$$

where

$$B = \frac{\delta D_s \gamma_{sv} \Omega}{RT}$$

and t = elapsed time, δD_s = surface thickness diffusivity product, γ_{sv} = solid–vapour interface energy, Ω = molar volume, R = gas constant and T = absolute and temperate.

The grain-boundary groove profile resulting from a lattice-diffusion mechanism is nearly the same as that resulting from surface diffusion. For the lattice-diffusion mechanism, the width between the peaks is given by [15]

$$w = 5(ct)^{1/3}$$

where

$$c = \frac{D_l \gamma_{sv} \Omega}{RT}$$

and D_l = lattice diffusivity.

The grain-boundary groove profile for the evaporation–condensation mechanism has no maxima and so can be distinguished from the lattice and surface diffusion mechanisms. The depth d of the grain-boundary groove caused by the evaporation–condensation mechanism is given by [14]

$$d = 1.13 c \tan\left(\frac{\phi}{2}\right)(At)^{1/2}$$

where

$$A = \frac{\alpha P^0 \gamma_{sv} \Omega^2}{(2\pi m)^{1/2}(RT)^{3/2}}$$

and ϕ is the dihedral angle, P^0 the pure metal vapour pressure, α the Langmuir condensation coefficient and m the atomic weight of the vapour-phase species.

Since the profiles for lattice and surface diffusion are similar, the growth rates are additive. If surface diffusion is the predominant mechanism, corrections for a small lattice-diffusion contribution can be applied in calculating the surface diffusivity as follows:

$$\delta D_s = \frac{RT}{\gamma_{sv} \Omega t}\left(\frac{w}{4.6}\right)^4 - 0.372 D_l w$$

The lattice-diffusion correction term was insignificant for the range of boundary widths examined.

The surface energy, γ_{sv} was assumed to be $1\,J\,m^{-2}$ for the purpose of calculating surface diffusivities. The surface energy is expected to be reduced with increasing temperature and solute segregation and chemisorption on the surface. The molar volume of silicon, Ω, was taken to be $12.06 \times 10^{-6}\,m^3\,mol^{-1}$. The gas constant R equals $8.3144\,J\,mol^{-1}\,K^{-1}$. The surface layer thickness δ is customarily taken as $\delta = \Omega^{1/3} = 2.714 \times 10^{-10}$ m if the surface diffusivity is reported separately from the δD_s product.

2.5. Sintering experiments

Model sintering experiments (sphere–sphere and sphere–plate) were conducted in the Brew vacuum

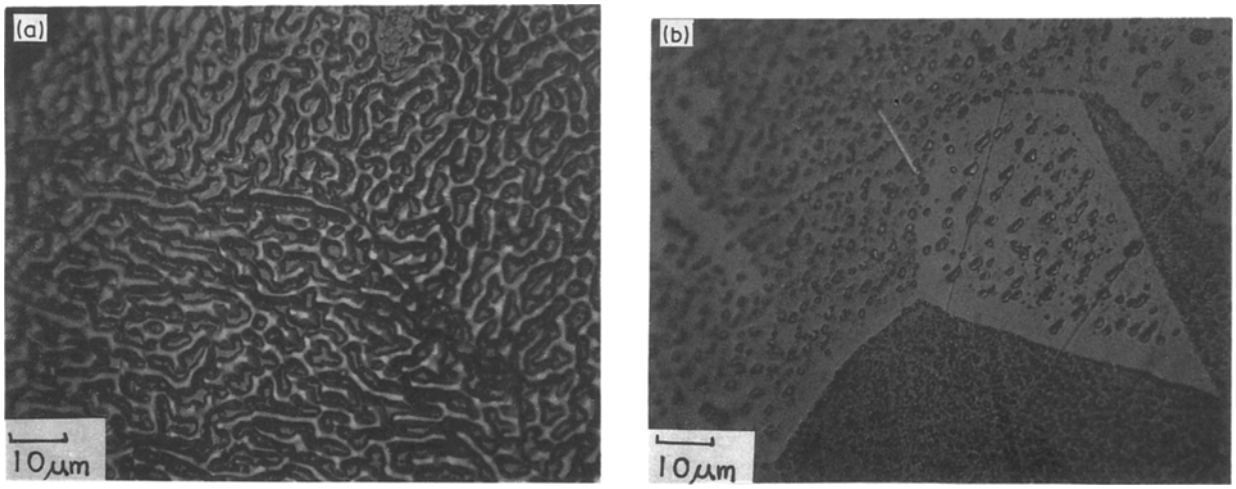

Figure 1 (a) Interface instability on freely evaporating boron-doped (0.2 wt %) silicon; (b) masked area of above sample.

furnace. Surface diffusivities were calculated from neck sizes using equations derived by Nichols and Mullins [16]. For sphere–sphere necks

$$\delta D_s = \frac{RTa^4}{25\gamma_{sv}\Omega t}\left(\frac{x}{a}\right)^6$$

where a = sphere radius and x = neck radius. For sphere–plate geometry

$$\delta D_s = \frac{RTa^4}{116\gamma_{sv}\Omega t}\left(\frac{x}{a}\right)^6$$

Grain-boundary grooves on the spheres or polycrystalline plates also may grow by surface diffusion. Since necks and grooves grow under the same experimental conditions of time, temperature and surface chemistry, the measurement of both groove width and neck size can be a sensitive measure of the ratio of mass transport coefficients. The following relations between the neck size and boundary profile width apply to sphere–sphere neck growth with surface diffusion as the dominant mechanism for grain-boundary grooving:

(a) If neck growth is dominated by surface diffusion

$$\left(\frac{x}{a}\right)^6 a^4/W^4 = 0.056$$

(b) If neck growth is dominated by grain-boundary diffusion

$$\left(\frac{x}{a}\right)^6 a^4/W^4 = 0.429\,\frac{wD_b}{\delta D_s}$$

where wD_b is the product of the grain boundary width and diffusivity.

(c) If grain-boundary diffusion is much faster than surface diffusion such that neck growth is controlled by surface redistribution [6] (SRCGBD)

$$\left(\frac{x}{a}\right)^7 a^4/W^4 = 0.404$$

3. Experimental results and discussion

3.1. Evaporation rate

Langmuir evaporation coefficients calculated from weight-loss measurements on one CVD pure silicon and five samples of polycrystalline boron-doped (0.2 wt % B) silicon at 1300° C show no significant difference between the doped and undoped samples. The average evaporation coefficient $\bar{\alpha}$ is 0.60.

Langmuir evaporation coefficients were also calculated from step-height measurements between 1100 and 1300° C. Six single-crystal samples with (1 1 1) orientation and one boron-doped sample resulted in values of α falling into two groups; low values of ~ 0.25 which may result from the mask lifting off the sample and allowing the reference plane to evaporate; and high values of 0.64 which is in agreement with the weight-loss measurements. Both high and low values could be measured on different parts of the same sample. No systematic variations were noted with temperature. Boron-doped samples were particularly hard to measure by this technique due to surface roughness which develops as a result of boron enrichment at the surface.

The Langmuir evaporation coefficients measured in this study fall within the range reported for pure silicon. Trulson and Schissel [17] report a value of 0.80 between 972 and 1060° C; Batdorf and Smits [18] report a value of 0.55 at 1300° C; Gulbransen *et al.* [19] report a value of 0.82 between 1100 and 1350° C; a value of 0.67 is calculated from Robertson's [5] evaporation rate at 1400° C and a value of 0.77 may be calculated from the evaporation rate reported by Nannichi [20].

3.2. Interface instability

Some early observations with boron-doped samples (Fig. 1) showed that the surface developed an undulating appearance as it evaporated. Evaporation of a two-component system has complexities not found in a one-component system. A second component may be either enriched or depleted in the surface region due to differing evaporation kinetics. Rough surfaces usually smooth out to minimize surface energy; however, in this case an initially smooth surface has developed roughness. The observation is related to the evaporation process, since part of the sample masked with a silicon shim to prevent free evaporation shows no roughening. The masked region is however pitted, especially at the grain boundaries and polishing scratches.

Boron can be expected to be enriched at the surface during evaporation since it has a much lower vapour pressure than silicon ($P_B^0/P_{Si}^0 = 10^{-4}$ at 1400° C). The process is analogous to solidification where solute is rejected at the liquid–solid interface and diffuses back into the liquid to form a solute-rich layer. For the case of evaporation, the vapour phase is growing into the solid and the solute is forced to diffuse back into the solid.

The surface roughness observed can be thought of as a surface instability analogous to that which arises from constitutional supercooling since the vapour pressure of the solvent, and hence the evaporation rate, is a function of both composition and curvature. If the solvent (silicon) is Raoultian and the solute (boron) is Henrian, then the vapour pressure of the solvent, P_{Si}, is given by

$$P_{Si} = P_{Si}^0 (1 - C_B)\left[1 + \left(\frac{\gamma_{sv}\Omega}{RT}\right)K\right]$$

where P_{Si}^0 is the vapour pressure of pure silicon, C_B is the atom fraction of boron and K is the surface curvature. The solid–vapour interface breaks down because the valleys and hills compensate negative and positive curvatures with lower and higher boron concentrations, respectively, such that the silicon vapour pressures and hence evaporation rates are equal. The implied boron concentration differences are consistent with the diffusion field that would result from the rough interface.

By analogy with constitutional supercooling [21] the zeroth-order approximation for the cell size is given by the ratio of the solute diffusivity, D_b, to the interface velocity, R. For the sample shown in Fig. 1, $R \approx 6.13 \times 10^{-8}$ cm sec^{-1} (calculated with an evaporation coefficient $\alpha = 0.62$) and $D_b = 2.53 \times 10^{-11}$ cm^2 sec^{-1} at 1300° C, which results in a cell size of 4.1 μm. This is in very good agreement with the wavelength observed on the sample ($\approx 4\,\mu$m). The wavelength of the interface instability is expected to be related to the boron boundary-layer thickness. If the surface concentration is pinned at C_s, the solubility limit, then the steady-state solution for the diffusion profile is given by

$$\frac{C - C_0}{C_s - C_0} = \exp\left(-\frac{RZ}{D_b}\right)$$

where C_0 is the bulk concentration and Z is the distance from the solid–vapour interface. The time required to reach steady-state conditions can be estimated from a mass balance on the solute. The excess boron in the solute-enriched layer is set equal to the boron from the evaporated region which assumes negligible vapour transport of boron. The time required to reach steady state is then given by

$$t = \frac{C_s - C_0}{C_0}\left(\frac{D_b}{R^2}\right)$$

The boron solubility limit at 1300° C as given by Armigliato *et al.* [22] is 0.39 wt %. The calculated time to reach steady-state conditions for the sample pictured in Fig. 1 is 0.83 h. Samples heat-treated for much longer times have boron-rich precipitates on the surface as determined with the scanning Auger microprobe.

By analogy with constitutional supercooling [23], high surface energy and/or rapid surface diffusion would be expected to suppress the interface instability or increase its wavelength. The complexities of the problem preclude a quantitative assessment of these effects. The interface instability is of significance because it points to the linkage of chemical and curvature driving forces. The implication for sintering is that each component must be transported in its stoichiometric ratio and that a minor component could be the rate-limiting species over shrinkage or coarsening paths. The good agreement between observed and calculated instability wavelengths indicates that the boron surface diffusivity is not large enough to be important, and this also is significant for sintering since it suggests that boron lattice diffusion may be the rate-limiting species over the coarsening path.

To test the hypothesis that boron lattice diffusion is the rate-controlling path for coarsening by surface diffusion, a diffusion couple was prepared between pure and boron-doped silicon. The details of this experiment can be found elsewhere [6]. This experiment provides a chemical driving force for surface transport as contrasted with a sintering or grain-boundary grooving experiment where mass transport is driven by gradients in surface curvature. If the silicon surface diffusivity were high, undercutting should be observed on the pure side of the couple due to a surface Kirkendall effect. Since no undercutting was observed, the conclusion is that boron lattice diffusion is not rate-controlling coarsening by surface diffusion, and the most likely role of boron is to reduce the silicon surface diffusivity.

3.3. Grain-boundary grooving experiments

Surface diffusivities calculated from grain-boundary groove widths are plotted in Fig. 2. The bulk of the data plotted in Fig. 2 fall either within the scatter band reported by Robertson [5] for pure silicon of below his least-squares fit by approximately an order of magnitude. The majority of the experiments were also carried out under experimental conditions for which Auger measurements indicate little boron surface segregation. Loss of boron from the surface can occur by several mechanisms. The equilibrium P_{O_2} at the silicon–silica phase boundary is approximately twelve orders of magnitude lower than the base pressure of the Brew vacuum furnace as noted in Fig. 3. The P_{O_2} within an oil diffusion-pumped vacuum system may be either reducing or oxidizing depending on the balance between back-streaming from the diffusion pump and air leaks into the chamber, respectively.

The reaction of silicon with SiO_2 produces high vapour pressures of SiO (Fig. 3). At P_{O_2} levels below the equilibrium P_{SiO} for this reaction, the oxygen impingement rate on the surface is balanced by the oxygen removal rate by SiO and active oxidative conditions prevail. Lander and Morrison's [24] LEED study of silicon indicates that this reaction determines the P_{O_2} against temperature boundary between atomically clean and oxidized surfaces. It can be expected

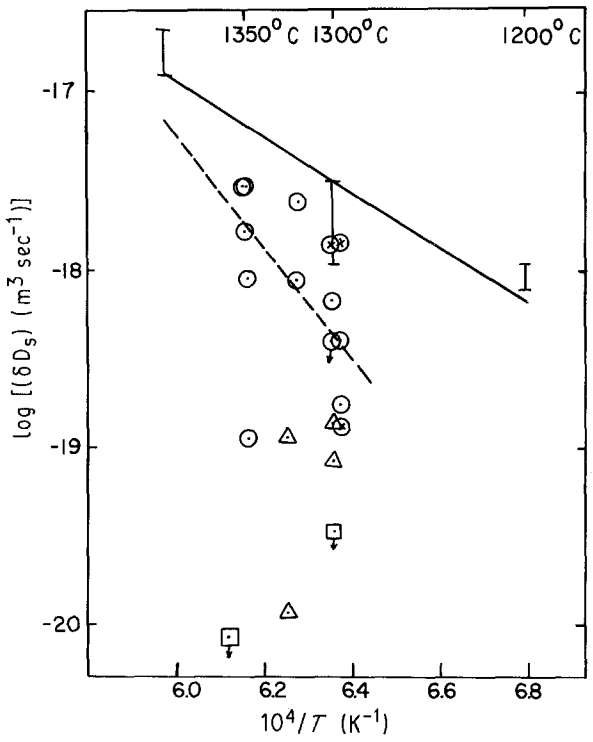

Figure 2 Surface diffusivities calculated from grain-boundary groove widths: (——) data of Robertson [5] for pure silicon; (⊙) 0.2 wt % B, (⊗) pure silicon, (△) silicon spheres, (⊡) 2 wt % B (molybdenum-lined Al_2O_3 tube, titanium-gettered argon).

that similar cleaning reactions are responsible for the removal of carbon and boron from silicon surfaces heat-treated in a vacuum. It should also be noted that the reaction of silicon with alumina will generate high vapour pressures of SiO and Al_2O.

Four samples, for which surface diffusivities were not calculated, exhibited anomalous grain-boundary groove profiles with excess matter at the grain-boundary surface intersection (Fig. 4). Auger analysis of one of these samples, originally doped with 0.2 wt % boron, had no detectable boron on external or fracture surfaces. The raised grain boundaries on this

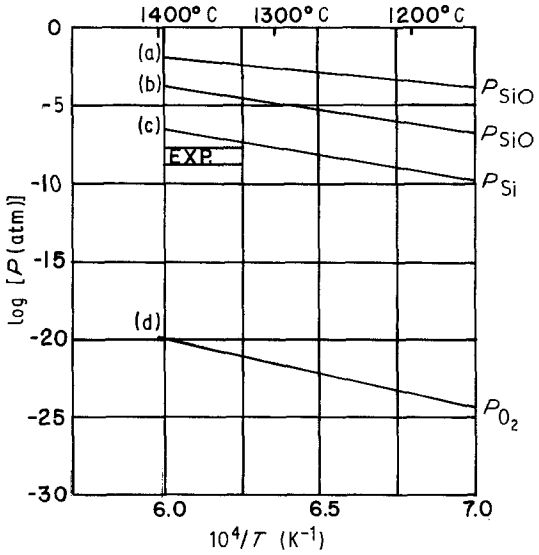

Figure 3 Pressure–temperature equilibrium reactions: (a) $Si + SiO_2 \rightarrow 2SiO$, (b) $2Si + Al_2O_3 \rightarrow Al_2O + 2SiO$, (c) silicon vapour pressure, (d) $Si + O_2 \rightarrow SiO_2$.

sample are evident in the two-beam interference micrograph and the low-angle back-scattered SEM micrograph shown in Fig. 4c. This sample was heat-treated under silicon powder which had been mixed with 0.2 wt % boron. The intention was to both pin the boron activity and prevent gross evaporation of the sample. However, oxygen associated with the silicon powder had the unexpected effect of leaching boron from the samples. Raised boundaries were found on one sample heat-treated without the silicon powder for which the vacuum system must have been sufficiently oxidizing to leach boron from the sample.

For the sample on which Auger measurements were made the effective diffusion depth calculated from the lattice diffusivity of boron in silicon is much too small to account for loss of boron in the bulk of the sample. The grain boundaries can act as a fast transport path, in which case the effective diffusion distance is half the grain size. Since boron occupies a substitution site in silicon and has a lattice diffusivity which is higher than silicon by a factor of approximately 40, a Kirkendall effect results as discussed by Bardeen and Herring [25]. Vacancies are injected into the lattice as a result of unequal boron and silicon fluxes. The climb of dislocations within the lattice maintains the vacancy concentration near its equilibrium value and gives rise to shrinkage of the sample since lattice sites are reduced. Condensation of vacancies at the grain boundary can lead to the formation of Kirkendall pores which were observed on a lightly etched cross-section. A grain-boundary Kirkendall effect can be expected if the boron grain-boundary diffusivity is greater than that of silicon. The degree to which grain-boundary grooves are raised above the surface depends upon both grain-boundary and lattice Kirkendall effects.

A general trend in the surface diffusivity data plotted in Fig. 2 is lower surface diffusivities with increased boron surface segregation as measured by Auger spectroscopy. For example, the lowest diffusivity plotted in Fig. 2 had an average boron concentration of 3 at %, boron-rich areas with up to 8 at %, and depleted areas of approximately 1.6 at %. It is also apparent from Auger measurements on boron-doped samples with high surface diffusivities that boron-thin surface films are easily leached from the surface under many experimental conditions.

3.4. Sintering experiments

The results of sintering experiments with pure silicon are listed in Table I. The low apparent diffusivities result from residual surface oxide layers, which results in an incubation time for surface smoothing as discussed by Munir [9]. Fig. 5 illustrates this point; some spheres have smooth surfaces and have begun to form necks, while spheres just below them appear pitted and unchanged from their as-received conditions. The surface oxide layer has presumably not yet peeled off the pitted spheres.

The surface diffusivities calculated from neck sizes were also low and in some cases much lower than those calculated from the grain-boundary groove widths on the same spheres. This apparent contradiction results from the effects of free evaporation in the vacuum.

TABLE I Model sintering experiments

Run No.	Treatment	Sample	Measurements	a (μm)	X (μm)	δD_s ($m^3 sec^{-1}$)	Remarks
1	2 h/1325° C	Spheres on silicon (1 1 1) single-crystal plate (sphere–plate geometry)	From SEM	128	5.3	1.79×10^{-21}	Low surface diffusivities calculated from neck size may be due to negative neck growth rates associated with evaporation.
				77	7.5	3.97×10^{-20}	
				91.5	4.3	9.97×10^{-22}	
				$w = 4.3\,\mu$m		1.12×10^{-19}	
2	8 h/1325° C $P_{system} = 10^{-6}$ torr	Spheres on silicon (1 1 1) single-crystal plate (sphere–sphere geometry)	From optical shadow graphs	86	7.80	4.66×10^{-20}	$(x/a)^6 a^4/w^4 = 0.18$ compared to 0.056 if surface diffusion; if grain-boundary diffusion $wD_b/\partial D_s = 0.415$.
				86	7.80	4.66×10^{-20}	
				119	8.80	5.02×10^{-20}	
				90	7.40	3.10×10^{-20}	
				90	5.85	7.57×10^{-21}	
			From SEM micrograph on a sphere	$w = 3.64\,\mu$m		3.64×10^{-20}	
						1.14×10^{-20}	
3	6 h 20 min/1300° C	Spheres in pile on boron-doped (2.0 wt %) silicon plate (sphere–sphere geometry)	From SEM	$x = 10\,\mu$m, $a = 70\,\mu$m		3.89×10^{-19}	$(x/a)^6 a^4/w^4 = 0.16$ compared to 0.056 predicted for surface diffusion.
				$w = 6.0\,\mu$m		1.38×10^{-19}	$(x/a)^7 a^4/w^4 = 0.023$ compared to 0.404 predicted for SRCGBD.
							If grain-boundary diffusion is the dominant neck growth mechanisms $wD_b/\delta D_s = 0.367$.
			From SEM	$x = 5.85\,\mu$m, $a = 80\,\mu$m		1.19×10^{-20}	Silicon spheres near top of pile; $(x/a)^6 a^4/w^4 = 0.0079$.
				$w = 5.3\,\mu$m		8.4×10^{-20}	

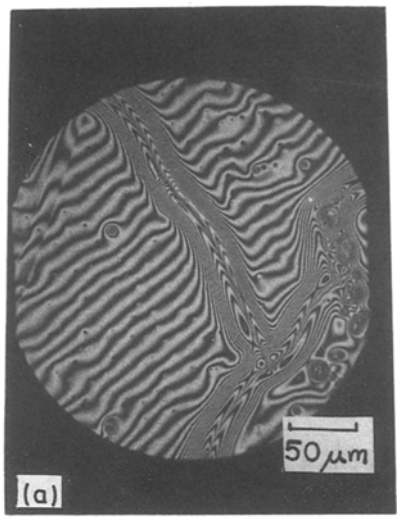

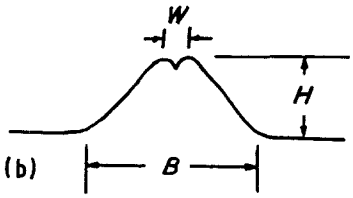

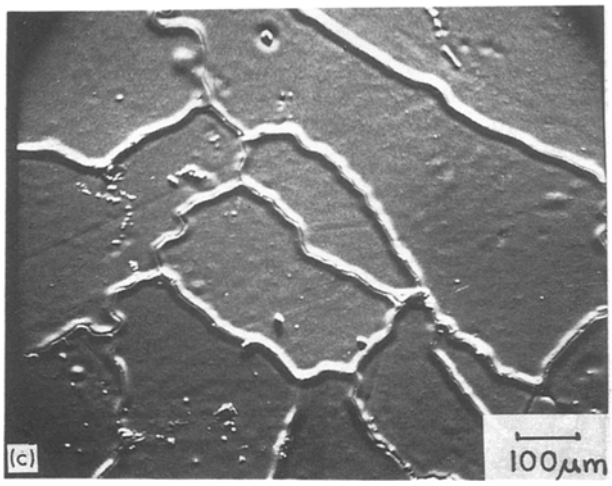

Figure 4 Raised grain-boundary grooves on sample: (a) two-beam interference micrograph; (b) groove profile schematic diagram ($W = 7.14\,\mu m$, $B = 35.7\mu m$, $H = 2.43\,\mu m$); (c) back-scattered SEM image of surface.

The relative saturation pressure of silicon determines the extent to which free evaporation occurs.

From examining neck sizes and grain-boundary groove widths on the spheres, the following tentative conclusions can be drawn for pure silicon:

1. Grain-boundary diffusion is not so fast that neck growth is rate-limited by surface redistribution. Since grain-boundary and surface diffusion mechanisms have the same particle size dependencies, this applies to all particle sizes.

2. Neck sizes are consistent with what should be expected for surface diffusion, but from these experiments a small contribution from grain-boundary diffusion cannot be ruled out.

3. The quantitative interpretation of silicon sintering experiments is clouded under free evaporation conditions by negative neck growth and, under condition where free evaporation is suppressed, by surface oxide films.

4. Spheres placed on the boron-doped plate (Table I, Run No. 3) did not form necks to the plate. Polishing scratches on the plate did not smooth significantly and apparent grain-boundary widths were less than 1 μm. This inhibition of sintering may have been related to either boron or residual surface oxide.

4. Initial-stage sintering map for silicon

The sintering map formalism introduced by Ashby [26] is ideally suited as a tool for displaying the competition between mechanisms during sintering. Understanding the competition between shrinkage and coarsening mechanisms, and the effect of additives on these competitions, is essential to understanding the sintering behaviour of silicon. The data and concepts introduced in previous sections will be brought together here and their effects on the shape of the sintering map will be discussed.

An isothermal initial-stage sintering map for silicon has been prepared (Fig. 6). A temperature of 1350° C was chosen for this map since the sintering experiments of Greskovich and Rosolowski [1] and much of

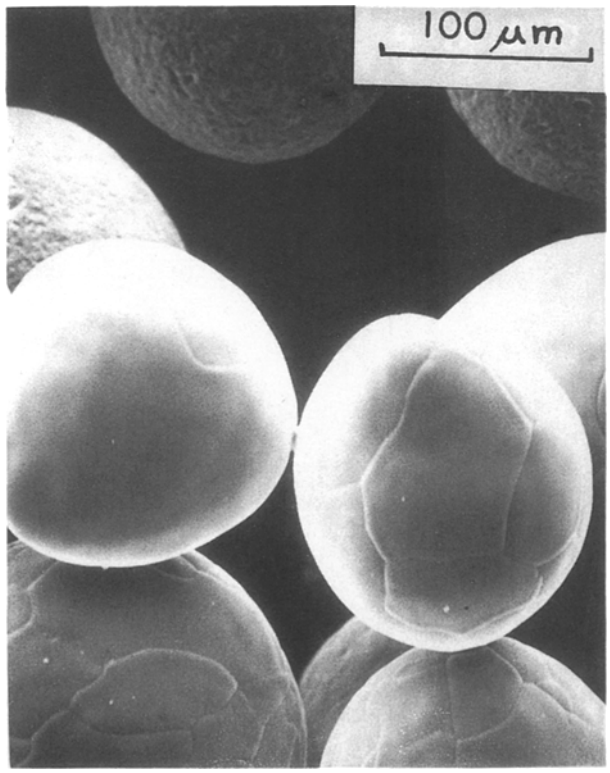

Figure 5 Silicon spheres near top of pile. ($6\frac{1}{3}$ h, 1300° C, surface smoothing and neck growth inhibited on pitted spheres near bottom of pile).

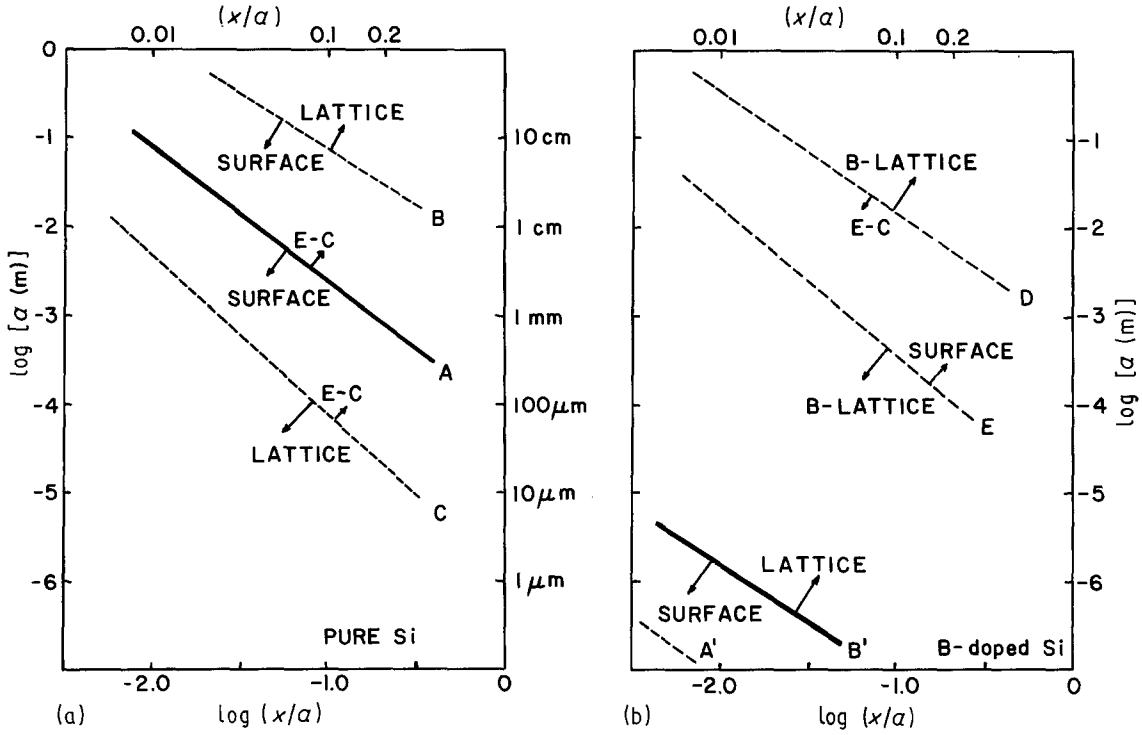

Figure 6 (a, b) Isothermal initial-stage sintering map for silicon.

the surface diffusion and evaporation rate measurements reported here apply to this temperature.

Lines where two mechanisms contribute equally are determined by equating the neck growth rates. The neck growth rate expressions listed in Table II were obtained by differentiating the initial stage models derived elsewhere [27]. The data base used and calculated neck growth rates may be found in Table III.

The effect of grain-boundary diffusion has not been included on the sintering map because data do not exist for it. The particle size dependency for the neck growth rate is the same for both grain-boundary and surface diffusion mechanisms. The neck growth data on pure silicon spheres indicate neck sizes compatible with surface diffusion. It is possible that a small contribution from grain-boundary diffusion would be undetected in the sphere–sphere neck growth experiments and still contribute to shrinkage. This small contribution, if it existed, would be independent of particle size and microstructure evolution, and would be characterized by much coarsening accompanying shrinkage.

TABLE II Neck growth rate expression evaluated at 1350° C*

$$\left(\frac{\dot{x}}{a}\right)_{\text{lattice}} = \frac{42.05\, D_2 \gamma_{sv} \Omega}{RTa^3}\left(\frac{x}{a}\right)^{-3.78}$$

$$= 5.59 \times 10^{-24}\ (\text{m}^3\ \text{sec}^{-1})\left(\frac{x}{a}\right)^{-3.78} \Big/ a^3$$

$$\left(\frac{\dot{x}}{a}\right)_{\text{surface}} = \frac{4.17\delta D_s \gamma_{sv} \Omega}{RTa^4}\left(\frac{x}{a}\right)^{-5}$$

$$= 2.38 \times 10^{-26}\ (\text{m}^4\ \text{sec}^{-1})\left(\frac{x}{a}\right)^{-5} \Big/ a^4$$

$$\left(\frac{\dot{x}}{a}\right)_{\text{vapour}} = \frac{2P^0_{Si}\gamma_{sv}\Omega^2}{(2\pi m)^{1/2}(RT)^{3/2}a^2}\left(\frac{x}{a}\right)^{-2}$$

$$= 4.39 \times 10^{-18}\ (\text{m}^2\ \text{sec}^{-1})\left(\frac{x}{a}\right)^{-2} \Big/ a^2$$

$$\left(\frac{\dot{x}}{a}\right)_{\substack{\text{boron lattice}\\ \text{coarsening}}} = \frac{5.95\, D_B \gamma_{sv} \Omega}{C_B RTa^3}\left(\frac{x}{a}\right)^{-3.33}$$

$$= 3.02 \times 10^{-21}\ (\text{m}^3\ \text{sec}^{-1})\left(\frac{x}{a}\right)^{-3.33} \Big/ a^3$$

*Data base listed in Table III.

The effect of boron on silicon grain-boundary diffusion is not known. One might expect boron to segregate to grain boundaries and lower the grain-boundary diffusivity for the same reasons that boron segregates to surfaces and lowers the surface diffusivity. If boron lowers the grain-boundary diffusivity by a smaller fraction than it lowers the surface diffusivity, then grain-boundary diffusion could dominate surface diffusion.

Referring now to the sintering map (Fig. 6) and calculated neck growth rates (Table III), the following is observed. For pure silicon the dominant mechanism below line A is surface diffusion. Above line A, vapour phase transport by the evaporation–condensation mechanisms dominates. Nowhere does a shrinkage mechanism dominate. Line C delineates the competition between evaporation–condensation and lattice diffusion and determines the second largest contribution to neck growth where surface diffusion is dominant. In a like manner, line B delineates the competition between surface diffusion and lattice diffusion and determines the second largest contribution to neck growth where evaporation–condensation is the dominant sintering mechanism.

A reduction of approximately six orders of magnitude in the surface diffusivity is needed to allow lattice diffusion to dominate sintering of submicrometre-sized powders. If we assume that boron is effective in reducing the surface diffusivity of silicon by six

TABLE III Silicon neck growth rates and data base for 1350° C

$\left(\frac{x}{a}\right)$	a (m)	$\left(\frac{\dot{x}}{a}\right)_{\text{lattice}}$ (sec^{-1})	$\left(\frac{\dot{x}}{a}\right)_{\text{surface(pure)}}$ (sec^{-1})	$\left(\frac{\dot{x}}{a}\right)_{\text{vapour}}$ (sec^{-1})	$\left(\frac{\dot{x}}{a}\right)_{\text{Boron lattice coarsening}}$ (sec^{-1})
0.01	10^{0}	2.03×10^{-16}	2.38×10^{-16}	4.39×10^{-14}	1.41×10^{-14}
	10^{-2}	2.03×10^{-10}	2.38×10^{-8}	4.39×10^{-10}	1.41×10^{-8}
	10^{-4}	2.03×10^{-4}	2.38	4.39×10^{-6}	1.41×10^{-2}
0.10	10^{-1}	3.37×10^{-17}	2.38×10^{-17}	4.39×10^{-14}	6.53×10^{-15}
	10^{-3}	3.37×10^{-11}	2.38×10^{-9}	4.39×10^{-10}	6.53×10^{-9}
	10^{-5}	3.37×10^{-5}	2.38×10^{-1}	4.39×10^{-6}	6.53×10^{-3}
0.20	10^{-1}	2.45×10^{-18}	7.44×10^{-19}	1.10×10^{-14}	6.48×10^{-16}
	10^{-3}	2.45×10^{-12}	7.44×10^{-11}	1.10×10^{-10}	6.48×10^{-10}
	10^{-5}	2.45×10^{-6}	7.44×10^{-3}	1.10×10^{-6}	6.48×10^{-4}
	10^{-7}	2.45	74.4×10^{5}	1.10×10^{-2}	6.48×10^{2}

$T_{Si} = 1623\,\text{K}$
$D_l = 1.49 \times 10^{-16}\,\text{m}^2\,\text{sec}^{-1}$ (silicon self-diffusivity) [28]
$\delta D_s = 6.39 \times 10^{-18}\,\text{m}^3\,\text{sec}^{-1}$ (pure silicon) [5]
$P^0_{Si} = 1.61 \times 10^{-2}\,\text{Nm}^{-2}$ [12]
$\Omega = 12.04 \times 10^{-6}\,\text{m}^3\,\text{mol}^{-1}$
$m = 2.81 \times 10^{-2}\,\text{kg mol}^{-1}$
$\gamma_{sv} = 1\,\text{J m}^{-2}$
$D_B = 5.71 \times 10^{-15}\,\text{m}^2\,\text{sec}^{-1}$ (boron diffusivity in silicon) [29]
$\alpha = 0.62$ (evaporation coefficient) (this study)
$R = 8.3144\,\text{J mol}^{-1}\,\text{K}^{-1}$ (gas constant)
$C_B = 0.01$ (atom fraction of boron assumed at 1350 K)

orders of magnitude, then lines B and A move to B′ and A′. For particle/neck size combinations above B′ and below C, lattice diffusion dominates and shrinkage occurs. Above line C coarsening by the evaporation–condensation mechanism dominates.

Additional inhibition of coarsening mechanisms may occur if boron becomes the rate-controlling species over the lattice path. Above line D, boron lattice diffusion controls the transport of silicon through the vapour phase. Below line E the boron lattice diffusion rate controls the transport of silicon by surface diffusion if the surface diffusivity of pure silicon is assumed. This line moves down one order of magnitude for each one order of magnitude in reduction of the surface diffusivity.

Boron lattice diffusion rate control of neck growth will always be greater than that due to lattice diffusion of silicon, since the boron diffusivity is larger and the total flux is enhanced by a factor of one divided by the atom fraction of boron. Thus, the fact that boron may become the rate-controlling species over the coarsening path will not lead to densification if the only shrinkage path is lattice diffusion. Densification may, however, occur by grain-boundary diffusion. If the grain-boundary diffusivity is large enough, neck growth may become controlled by either boron lattice diffusion or surface redistribution control of boron with fast transport of silicon by grain-boundary diffusion.

5. Conclusions and discussion

The particle size dependency for shrinkage of pure silicon compacts found by Greskovich and Rosolowski [1] and their interpretation of vapour transport as the dominant coarsening mechanism is inconsistent with the grain-boundary diffusivity measurements of Robertson [5] and this study, which indicates that surface transport should be the dominant coarsening mechanism at all particle sizes of interest. The inconsistency is removed if we consider the role of oxygen in the sinterability of pure silicon. Thin oxide layers inhibit surface diffusion and allow competing densification mechanisms (grain-boundary or lattice) to dominate the sintering of ultrafine silicon compacts. The slower shrinkage rate associated with larger particle sizes allows oxygen to be leached from the compact as SiO. At intermediate particle sizes, oxygen is partially removed resulting in surface-dominated coarsening while the interior of the compact is dominated by shrinkage mechanisms. Möller and Welsch [8] observed porous surface regions on their sintered pellets. Oxygen is thus a sintering aid for silicon which acts to inhibit surface diffusion. Methods to conserve oxide surface layers, such as powder beds of silicon + SiO_2 to generate equilibrium SiO vapour pressures, should be used to densify silicon powder compacts with larger particle sizes than those reported in the literature.

The Herring's scaling law argument of Greskovich and Rosolowski [1] is deceptive because the surface diffusivity is strongly affected by thin oxide layers and the stability of the oxide layers is sensitive to time at temperature, particle size, and the presence of other impurities such as iron.

Boron is also an effective sintering aid for silicon because it inhibits the surface diffusivity. The leaching of boron from silicon compacts under active oxidation conditions can result in unusual raised grain-boundaries. Free evaporation of boron-doped silicon resulted in an unexpected solid–vapour interface instability. The combination of these two effects complicated the experimental aspects of this study greatly.

Acknowledgements

This work was funded by the Department of Energy, Contract Number DE-ACO2-76 ERO2390 and comprises the thesis work of the author which was supervised by Professors R. L. Coble and R. M. Cannon at the Massachusetts Institute of Technology. The technical assistance of Mr Pat Kearney, Mr Al Frecker, Mr Cliff Herman and Mr Art Gregor, all of MIT, is gratefully acknowledged. Discussions with Drs S. Prohazka and C. Greskovich of G. E. stimulated the onset of this study. Thanks are also due to Mrs Janice Lemley of Norton Co. for typing this manuscript.

References

1. C. GRESKOVICH and J. R. ROSOLOWSKI, *J. Amer. Ceram. Soc.* **59** (7-8) (1976) 336.
2. C. GRESKOVICH, J. R. ROSOLOWSKI and S. PROHAZKA, "Ceramic Sintering", Final Technical Report, ARPA Order No 2698 (SRD-75-084) (US Government Printing Office, 1975).
3. C. GRESKOVICH, *J. Mater. Sci.* **16** (1981) 613.
4. J. S. HAGGERTY, Massachusetts Institute of Technology, personal communications (1980).
5. W. M. ROBERTSON, *J. Amer. Ceram. Soc.* **64** (1) (1981) 9.
6. W. S. COBLENZ, PhD Thesis, Massachusetts Institute of Technology (1981).
7. N. J. SHAW and A. H. HEUER, *Acta Metall.* **31** (1983) 55.
8. H. MÖLLER and G. WELSCH, *J. Amer. Ceram. Soc.* **68** (6) (1985) 320.
9. Z. A. MUNIR, *J. Mater. Sci.* **14** (1979) 2733.
10. S. M. BOYER and A. J. MOULSON, *ibid.* **13** (1978) 1637.
11. L. E. DAVIS *et al.*, "Handbook of Auger Spectroscopy", 2nd Edn (Physical Electronics Industries Inc., 1976).
12. D. R. STULL and H. PROPHET, "Diffusion Mechanisms and Point Defects in Silicon and Germanium", JANAF Thermochemical Tables, 2nd Edn (National Bureau of Standards, Washington, DC, 1971).
13. J. M. DYNYS, Massachusetts Institute of Technology, Personal Communication (1979).
14. W. W. MULLINS, *J. Appl. Phys.* **28** (1957) 333.
15. *Idem*, *AIME Trans.* **218** (1960) 354.
16. F. A. NICHOLS and W. W. MULLINS, *J. Appl. Phys.* **36** (1965) 1826.
17. O. C. TRULSON and P. O. SCHISSEL, in Proceedings of Symposium on Condensation Evaporation Solids, Dayton, Ohio, 1962 (1974) pp. 313–317.
18. R. L. BATDORF and F. M. SMITS, *J. Appl. Phys.* **31** (1959) 259.
19. E. A. GULBRANSEN, K. F. ANDREW and F. A. BRASSART, *J. Electrochem. Soc.* **113** (1966) 834.
20. Y. NANNICHI, *Jpn J. Appl. Phys.* **2** (1963) 586.
21. W. A. TILLER *et al.*, *Acta Metall.* **1** (1953) 428.
22. A. ARMIGLIATO *et al.*, in "Semiconductor Silicon 1977", edited by H. Huff and E. Sirtl, (The Electrochemical Society, 1977) p. 638.
23. G. F. BOLLING and W. A. TILLER, *J. Appl. Phys.* **31** (1960) 2040.
24. J. J. LANDER and J. MORRISON, *ibid.*, **33** (1962) 2089.
25. J. BARDEEN and C. HERRING, in "Imperfections in Nearly Perfect Crystals", edited by W. Shockley (Wiley, New York, 1952) p. 261.
26. M. F. ASHBY, *Acta Metall.* **22** (1974) 275.
27. W. S. COBLENZ *et al.*, in "Sintering Processes", Material Science Research Vol. 13, edited by G. C. Kuczynski, (Plenum, New York, 1980) pp. 141–157.
28. I. R. SANDERS and P. S. DOBSON, *J. Mater. Sci.* **9** (1974) 1987.
29. A. SEEGER and K. P. CHIK, *Phys. Status Solidi*, **29** (1968) 455.

Received 22 March
and accepted 4 September 1989